Journal of Alloys and Compounds 488 (2009) 195–198

Contents lists available at ScienceDirect

Journal of Alloys and Compounds

journal homepage: www.elsevier.com/locate/jallcom

Pt_xNi alloy nanoparticles as cathode catalyst for PEM fuel cells with enhanced catalytic activity

Huimin Wu, David Wexler, Guoxiu Wang*

Institute for Superconducting & Electronic Materials, School of Mechanical, Materials and Mechatronics Engineering, University of Wollongong, Wollongong, NSW 2522, Australia

ARTICLE INFO

Article history:
Received 19 June 2009
Received in revised form 14 August 2009
Accepted 14 August 2009
Available online 25 August 2009

Keywords:
Cathode catalyst
PEM fuel cell
Oxygen reduction reaction
Pt–Ni alloys

ABSTRACT

A series of Pt_xNi/C ($x = 1–3$) nanoparticle catalysts were prepared using a chemical reduction method, where the aim was to reduce the Pt loading and maintain high catalytic reactivity towards the oxygen reduction reaction. The catalysts were characterized by X-ray diffraction, field emission scanning electron microscopy, and transmission electron microscopy. The electrochemical performance of the Pt_xNi/C alloy catalysts was evaluated by cyclic voltammetry, steady-state measurements, and chronoamperometric testing. We found that the catalytic reactivity of Pt catalysts towards oxygen reduction can be maintained or even enhanced by partially replacing platinum with nickel.

1. Introduction

Proton exchange membrane fuel cells (PEMFCs) are a class of devices used for the conversion of chemical energy into electrical energy [1]. Recently, they have aroused great interest in both academic and industrial research due to their high efficiencies and ability to operate without greenhouse gas emissions [2,3]. Furthermore, PEM fuel cells can be operated at relatively low temperatures (under 120 °C) [4].

Noble metals, such as Pt supported on high surface area carbons, are typically used as electrocatalysts for PEM fuel cells [5–7]. The resultant high cost is one of the obstacles preventing the popular usage of PEM fuel cells. In order to reduce costs, one method is to prepare Pt nanoparticles supported on carbon, which helps to lower the platinum loading in the PEM fuel cells [8,9]. Another approach is to synthesize platinum-based binary or ternary electrocatalysts. As example, Ru [10,11], Mo [12], and Cu [13] have been used as catalysts together with Pt. There is increasing interest in the Pt–Ni alloys, because of their lower material cost and effective resistance to electrolyte dissolution. It has been reported that Pt_xNi alloys are promising catalysts for the oxygen reduction reaction (ORR) [14–20].

In this paper, we synthesized a series of Pt_xNi ($x = 1–3$) alloy nanoparticles on carbon matrix. Although these Pt_xNi alloy catalysts contain a reduced content of Pt, they exhibit significantly enhanced catalytic activity towards oxygen reduction compared to pure platinum catalyst. Our results show great promise for a solution to the problem of high demand for platinum in the cathode catalysts in current PEM fuel cells.

2. Experimental

2.1. Preparation and deposition of Pt_xNi catalyst nanoparticles

To prepare nanosized Pt_xNi alloys, a mixture of $NiCl_2 \cdot 6H_2O$ (Aldrich, 99.9%) and $H_2PtCl_6 \cdot 6H_2O$ (Aldrich, 99.9%) was dissolved in de-ionized water with the Pt:Ni (atomic ratio) = 1:1, 2:1, and 3:1, respectively. Then an appropriate amount of carbon (Vulcan XC-72; Pt_xNi:C (weight ratio) = 20:80) was added to the solution and dispersed by ultrasonic probe for about 0.5 h (Brandson Ultrasonifier, 35% amplitude). After that, each solution was heated in an oil bath to 138 °C at which point 10 mL aqueous solution of superfluous $NaBH_4$ was added dropwise into the mixture for reduction under Ar atmosphere. The reacting dispersion was stirred and refluxed continuously for at least 30 min and then cooled down to room temperature. Finally, the black dispersion was isolated by centrifugation and washed 3–4 times with ethanol. The black powder was then dried at 60 °C in a vacuum oven overnight. A sample of Pt (20 wt%) on Vulcan XC-72 was also prepared by a similar procedure for comparison.

2.2. Structural characterization

X-ray diffraction patterns were obtained with a GBC MMA X-ray diffractometer with Cu Kα radiation. The morphologies and distributions of platinum and Pt–Ni alloy nanoparticles supported on Vulcan XC-72 carbon were investigated by field emission gun scanning electron microscopy (FEG-SEM) using a JEOL 7001F instrument, with additional semi-quantitative information obtained using large area standardless energy dispersive X-ray spectroscopy (EDX) analysis. Transmission electron microscopy (TEM) was performed using a JEOL JEM 2011 TEM facility. TEM specimens were prepared by making a suspension of catalyst powder in ethanol and depositing a drop of the suspension on a standard carbon-covered copper grid.

* Corresponding author. Tel.: +61 2 42215726; fax: +61 2 42215731.
E-mail address: gwang@uow.edu.au (G. Wang).

0925-8388/$ – see front matter © 2009 Elsevier B.V. All rights reserved.
doi:10.1016/j.jallcom.2009.08.077

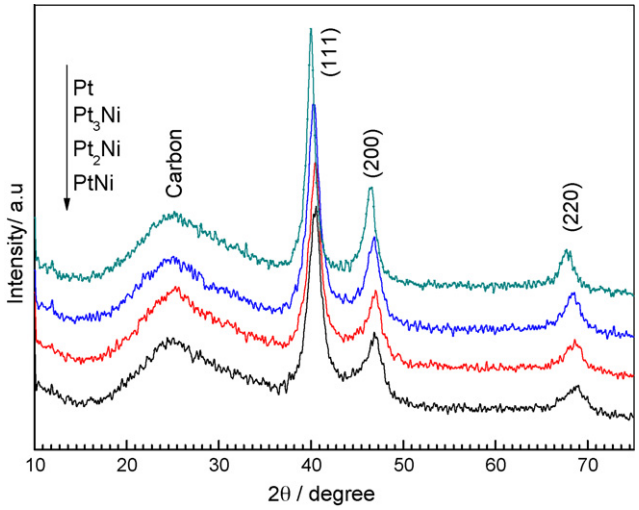

Fig. 1. X-ray diffraction patterns of Pt_xNi catalyst nanoparticles deposited on Vulcan XC-72 carbon matrix.

2.3. Electrochemical testing

Electrochemical measurements were performed with a three-electrode configuration. The working electrodes were made by casting carbon-supported nanoparticles (Pt_xNi/C or Pt/C) as a thin film onto a glass carbon rotating disk electrode with Nafion as a binding agent. The counter electrode was a Pt foil, and the reference electrode was a saturated calomel electrode. So all potentials are reported with respect to the saturated calomel electrode (SCE) throughout the paper. The electrolyte solution was 0.5 mol/L H_2SO_4. Electrochemical measurements were performed using a glassy carbon rotating disk electrode (RDE, model AFMSRCE, Pine Research Instrumentation) connected to a bipotentiostat (AFCBPIE, Pine Research Instrumentation).

3. Results and discussion

Fig. 1 shows the X-ray diffraction patterns of Pt_xNi alloys and Pt catalysts deposited on Vulcan XC-72 carbon. The XRD of pure nickel is characterized by three diffraction peaks at $2\theta = 44.5^\circ$ (1 1 1), 51.8° (2 0 0), and 76.4° (2 2 2), while that of fcc Pt by peaks at $2\theta = 39.9^\circ$ (1 1 1), 46.2° (2 0 0), and 67.9° (2 2 0). Therefore, the diffraction peaks at 40°, 46°, and 68° in Fig. 1 display primarily the characteristics of fcc Pt without any trace of fcc Ni [21]. Apart from the three strong diffraction peaks of platinum, another broad diffraction peak at about 24° represents amorphous carbon. We noted that the major diffraction peaks of Pt_xNi catalysts are gradually shifted to higher 2θ angles with increasing Ni content. This indicated a contraction of the lattice and confirmed the formation of Pt–Ni alloys due to the incorporation of Ni into the fcc structure of Pt. No characteristic diffraction peaks of metallic or Ni oxides were detected, indicating that the oxidation of Ni can be effectively prevented by the use of flowing argon gas in the reduction process. The diffraction peaks of the as-prepared Pt_xNi alloy catalysts were broader than those of Pt, which can be attributed to the smaller crystallite sizes of those alloy catalysts.

Table 1 shows the values of the lattice parameters and the mean crystallite size of all the catalysts determined quantitatively from XRD analysis. It can be seen that the crystallite sizes and lattice parameters of the alloy catalysts decrease with increasing Ni content, which is in good agreement with the above analyses. This can be attributed to that more Ni can enter into the lattice of Pt with increasing Ni content, which has also been reported in the previous research [22].

Table 1
Average crystallite sizes and lattice parameters determined by XRD.

Sample	Crystallite size (nm)	Lattice parameter (Å)
Pt	5.90	3.90
Pt_3Ni	2.68	3.89
Pt_2Ni	2.36	3.86
PtNi	2.32	3.87

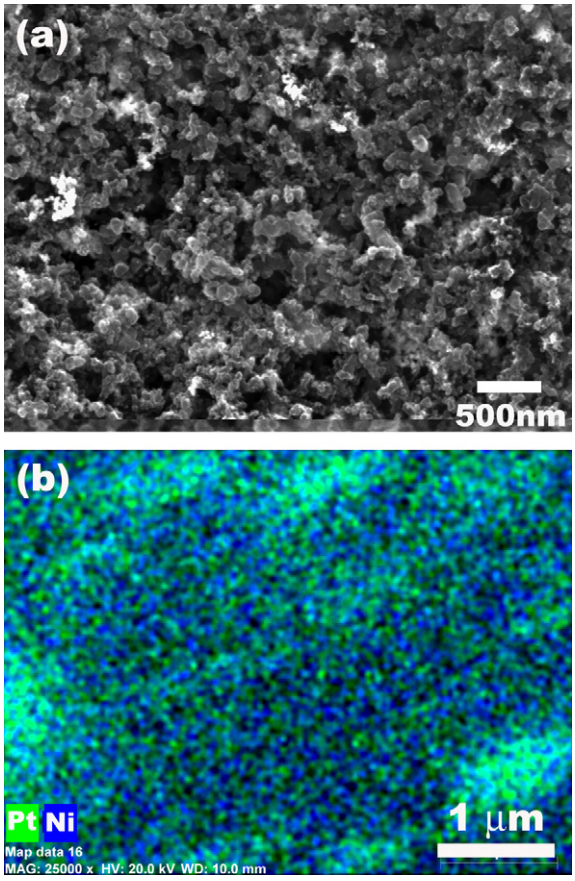

Fig. 2. (a) FEG-SEM image of Pt_2Ni catalyst nanoparticles deposited on an Vulcan XC-72 carbon matrix. (b) Back-scattering element mapping of Pt and Ni, showing homogeneous distribution of alloy element.

The morphologies of the as-prepared Pt_xNi alloy catalysts deposited on Vulcan XC-72 carbon matrix were observed by FEG-SEM. Fig. 2(a) shows a SEM image of a typical Pt_2Ni alloy catalyst. In general the carbon matrix exhibits a fluffy cotton-like microstructure, in which Pt_2Ni alloy catalyst nanoparticles are embedded. We performed quantitative EDX analysis. For each sample, the Pt:Ni atomic ratio was equal to the nominal ratio. The distributions of Pt_2Ni in the carbon matrix were examined by back-scattering elemental mapping (as shown in Fig. 2(b)), from which we can see that Pt and Ni are distributed homogeneously on the micrometer domain.

Fig. 3(a) and (b) shows bright-field TEM images of PtNi/carbon and Pt/carbon catalysts, respectively. The dark nanoparticles are the PtNi or Pt catalysts. We performed selected area electron diffraction (SAED) on the catalysts. The associated spotty ring patterns are shown in the insets in Fig. 3(a) and (b), respectively. The bright spots on the SAEDs correspond to the (1 1 1) and (2 0 0) Pt reflections, and the additional diffuse rings correspond to amorphous carbon. It also can be seen that the catalyst particles have a particle size in the range of a few nanometers, which is consistant with the results deduced from XRD.

The electrochemical performance of catalyst materials is very sensitive to their surface composition and structures. Cyclic voltammetric (CV) responses of the as-prepared electrocatalysts in 0.5 mol/L H_2SO_4 electrolyte are presented in Fig. 4. The current val-

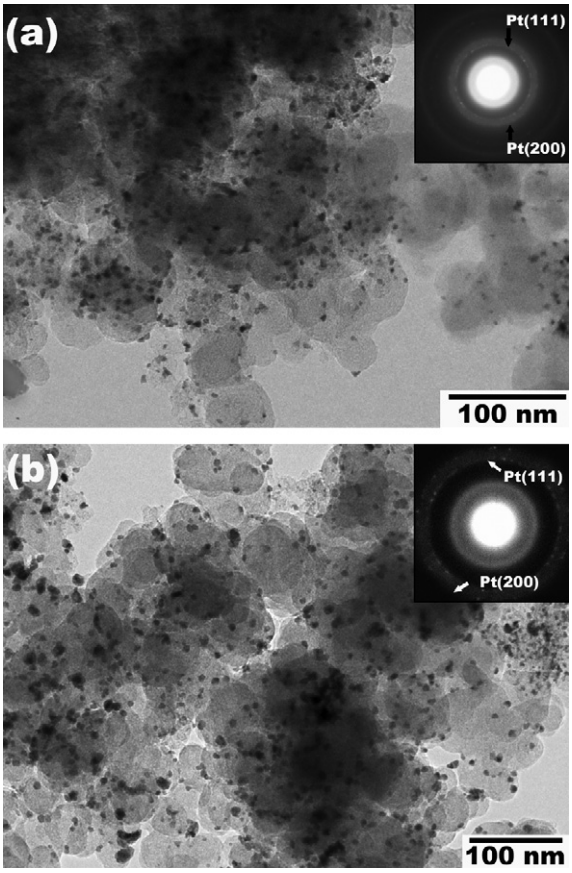

Fig. 3. Bright-field TEM image of Pt_xNi/carbon catalysts. The insets are the corresponding selected area electron diffraction patterns. (a) PtNi/carbon. (b) Pt/carbon.

ues were normalized per milligram of platinum. We can see that all CV curves have an obvious hydrogen adsorption–desorption region of −0.25 to 0.1 V *vs.* SCE, and the current peak associated with the reduction of platinum oxide is in the region of 0.4–0.55 V *vs.* SCE, indicating the electrochemically active nature of the as-prepared nanosize Pt_xNi catalysts. The cathodic current peaks associated

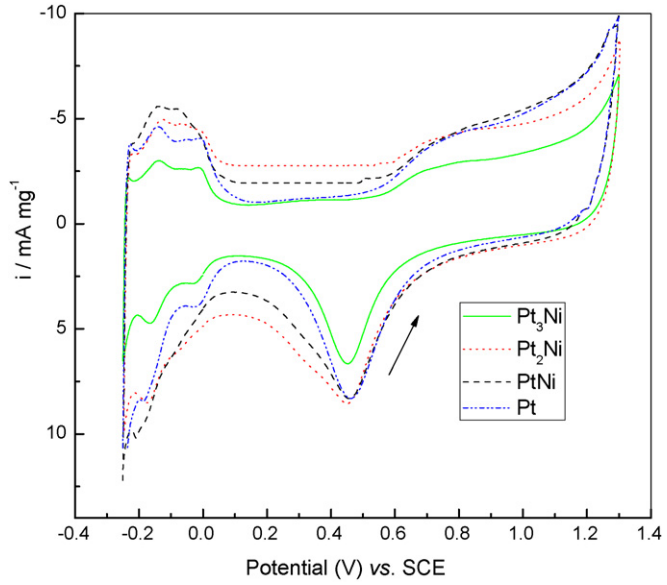

Fig. 4. Cyclic voltammograms of Pt_xNi/carbon catalysts in argon-saturated 0.5 mol/L H_2SO_4 electrolyte. Scanning rate: 50 mV/s.

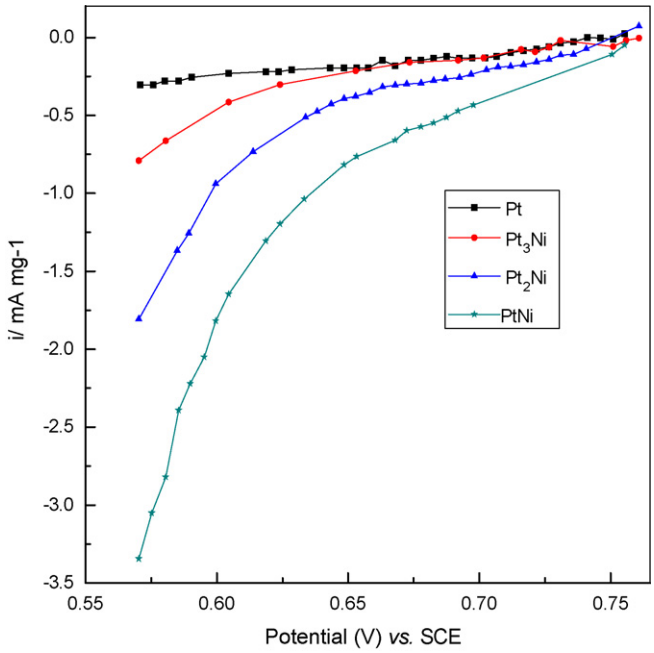

Fig. 5. Catalytic activities toward the oxygen reduction reaction measured by rotating the electrodes at 1600 rpm.

with the reduction of platinum oxide positively shift more than 5 mV for the Pt_3Ni and Pt_2Ni catalysts, and about 15 mV for the PtNi catalyst, as compared to the pure Pt catalyst. This implied that the desorption of the oxygenate species (e.g., OH) from the surfaces of the alloy particles is easier than from the surface of Pt, i.e., the oxygenate species have a lower adsorption energy on the Pt_xNi alloy catalysts. This phenomenon has also been observed by Markovic and co-workers [23–27]. Since the adsorption of OH (or other oxygenate species) on Pt surface can inhibit its catalytic activity toward ORR, the weak adsorption of the oxygenated species would increase the surface active sites for ORR.

Furthermore, all the CV curves have the same shape, implying that Pt atoms represent the main active sites for the oxidation reaction. The reaction mechanism of oxygen reduction on platinum can be interpreted as follow [28]:

$$O_2 + Pt \rightarrow Pt\text{–}O_2 \quad (1)$$

$$Pt\text{–}O_2 + H^+ + e^- \rightarrow Pt\text{–}HO_2(ads) \quad (2)$$

$$Pt\text{–}HO_2 + Pt \rightarrow Pt\text{–}HO + Pt\text{–}O \quad (3)$$

$$Pt\text{–}HO + Pt\text{–}O + 3H^+ + 3e^- \rightarrow 2Pt + 2H_2O \quad (4)$$

Therefore, the enhanced electrocatalytic activity of the Pt_xNi electrode may be attributed to two factors: One is the increase in electroactive platinum species, caused by the introduction of nickel [29]. In other words, Ni can facilitate the desorption of the oxygenate species (e.g., OH) from the surfaces of alloy particles. Because Ni has a lower electronegativity than Pt, which can be attributed to a change in the electronic properties of Pt. The other is that the incorporation of Ni into the fcc structure of Pt induces contraction of the lattice. The contraction can sensitively lead to a change in the electronic properties of platinum which weakens the strength of the M–O bond. Both of these two factors can increase the speed of the above reactions, so Pt_xNi alloy catalysts demonstrate better electrocatalytic activity. Furthermore, as the Ni content increases, the effects will be enhanced. Among all the prepared catalyst samples, PtNi catalyst exhibits the highest electrochemical reactivity.

Fig. 5 shows the results of catalytic activity for the ORR on different catalysts. Obviously, the catalytic activities for the ORR on

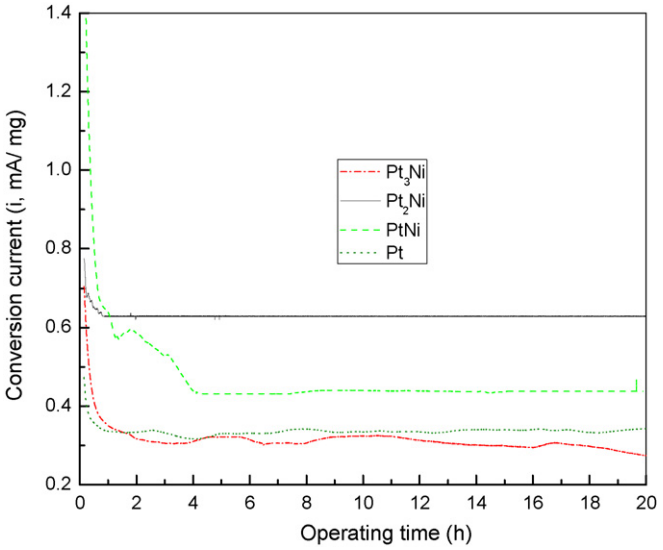

Fig. 6. Chronoamperometric curves of Pt_xNi/carbon catalysts in oxygen-saturated 0.5 mol/L H_2SO_4, measured at 0.6 V *vs.* SCE.

Pt_xNi are higher than that on pure Pt particles. PtNi shows the highest catalytic activity, followed by Pt_2Ni, Pt_3Ni and Pt, agreeing with the positive shift of the oxide reduction peak in the CV. Since the oxygen reduction reaction (ORR) on Pt surfaces has slow kinetics, it is responsible for the overpotential losses of ~0.3–0.4 V under typical conditions of operation [30]. However, alloying platinum with other first-row transition metals such as Ni can effectively reduce the overpotential and therefore, enhance the current density.

Since the cathode in a fuel cell is exposed to the corrosive environment of the acidic electrolyte and oxygen, the stability of the alloy catalysts must be studied. For this purpose, chronoamperometry tests in 0.5 mol/L H_2SO_4 with saturated oxygen were conducted. Fig. 6 shows the chronoamperometry curves at the constant potential of 0.60 V. In spite of the initial high current density, there is a rapid decay in the initial period of time. After 4 h operation, the ORR reduction currents were gradually stabilized for all of the catalysts. The PtNi and Pt_2Ni catalysts showed much higher conversion currents than the Pt_3Ni and Pt catalysts. Therefore, the results of all the electrochemical testing indicated that PtNi and Pt_2Ni alloy catalysts had better electrochemical performances towards ORR than that of the pure Pt catalyst.

4. Conclusion

Nanosize Pt_xNi ($x = 1–3$) catalysts on carbon matrix were prepared by a chemical reduction method. The as-prepared catalysts have a uniform distribution on the carbon matrix, with a particle size in the range of 3–5 nm. Electrochemical testing results indicate that the presence of Ni enhances the electrocatalytic activity and long-term stability of the catalysts. Our results show that the prepared Pt_xNi alloy nanoparticles could have promising applications in PEM fuel cells as effective catalysts for oxygen reduction, with the added feature of reduced cost due to lower Pt loading.

Acknowledgements

We are grateful for financial support from the Australian Research Council (ARC) through an ARC Linkage project entitled "Exploration of new catalyst materials for hydrogen/air fed proton exchange membrane fuel cells" (LP0775109).

References

[1] E. Negro, V.D. Noto, J. Power Sources 178 (2008) 634.
[2] S. Hirano, J. Kim, S. Srinivasan, Electrochim. Acta 42 (1997) 1587.
[3] V.A. Paganin, E.A. Ticianelli, E.R. Gonzalez, J. Appl. Electrochem. 26 (1996) 297.
[4] A. Heinzel, C. Hebling, in: W. Vielstich, A. Lamm, H.A. Gasteiger (Eds.), Fuel Cells-fundamentals, Technology and Applications, John & Sons, Hoboken, NJ, 2003, p. 1142.
[5] B. Goodenough, A. Hamnett, B.J. Kennedy, R. Manoharan, S.A. Weeks, J. Electroanal. Chem. 240 (1998) 133.
[6] P. Hogarth, T.R. Ralph, Platinum Met. Rev. 46 (2002) 146.
[7] Y. Mu, H. Liang, J. Hu, L. Jiang, L. Wan, J. Phys. Chem. B 109 (2005) 22212.
[8] M.S. Saha, A.F. Gulla, R.J. Allen, S. Mukerjee, Electrochim. Acta 51 (2006) 4680.
[9] M.S. Wilson, S. Gottesfeld, J. Electrochem. Soc. 139 (1992) 28.
[10] J.H. Choi, K. Park, B. Kwon, Y. Sung, J. Electrochem. Soc. 150 (2003) A973.
[11] S.A. Lee, K. Park, J. Choi, B.K. Kwon, Y.E. Sung, J. Electrochem. Soc. 149 (2002) A1299.
[12] K.W. Park, J.H. Choi, B.K. Kwon, S.A. Lee, Y.E. Sung, J. Phys. Chem. B 106 (2002) 1869.
[13] K.W. Park, J.H. Choi, S.A. Lee, C. Park, H. Chang, Y.E. Sung, J. Catal. 224 (2004) 236.
[14] P.V. Samant, J.B. Fernandes, J. Power Sources 125 (2004) 172.
[15] G. Samjeske, H. Wang, T. Loffler, H. Baltruschat, Electrochim. Acta 47 (2002) 3681.
[16] P. Minyukova, T.I. Simentsova, A.V. Khasin, N.V. Shtertser, N.A. Baronskaya, A.A. Khassn, T.M. Yurieva, Appl. Catal. A 237 (2002) 171.
[17] T.C. Deivaraj, W. Chem, J.Y. Lee, J. Mater. Chem. 13 (2003) 2555.
[18] A. Lima, C. Coutanceau, J.M. Leger, C. Lamy, J. Appl. Electrochem. 31 (2001) 379.
[19] F. Liu, J.Y. Lee, W. Zhou, J. Phys. Chem. A 108 (2004) 17959.
[20] K.W. Park, J.H. Choi, Y.E. Sung, J. Phys. Chem. B 107 (2003) 5851.
[21] T.C. Deivaraj, W. Chen, J.Y. Lee, Materials 13 (2003) 2555.
[22] L. Xiong, A.M. Kannan, A. Manthiram, Electrochem. Commun. 4 (2002) 898.
[23] V.R. Stamenkovic, B. Fowler, B.S. Mun, G.F. Wang, P.N. Ross, C.A. Lucas, N.M. Markovic, Science 315 (2007) 493.
[24] V. Stamenkovic, T.J. Schmidt, P.N. Ross, N.M. Markovic, J. Phys. Chem. B 106 (2002) 11970.
[25] V. Stamenkovic, T.J. Schmidt, P.N. Ross, N.M. Markovic, J. Electroanal. Chem. 191 (2003) 554.
[26] V.R. Stamenkovic, B.S. Mun, K.J.J. Mayrhofer, P.N. Ross, N.M. Markovic, J. Am. Chem. Soc. 128 (2006) 8813.
[27] M.H. Shao, K. Sasaki, R.R. Adzic, J. Am. Chem. Soc. 128 (2006) 3526.
[28] K. Hiroshima, T. Asaoka, T. Noritale, Y. Ohya, Y. Morimoto, Fuel Cells 2 (2002) 31.
[29] T.C. Wen, C.H. Hu, C.C. Hu, J. Chin. Inst. Chem. Eng. 30 (1999) 515.
[30] H.A. Gasteiger, W. Gu, R. Makharia, M.F. Mathias, B. Sompalli, in: W. Vielstich, A. Lamm, H.A. Gasteiger (Eds.), Fundamentals, Technology and Applications, vol. 3, Wiley, New York, 2003 (chapter 46).